Accepted Manuscript

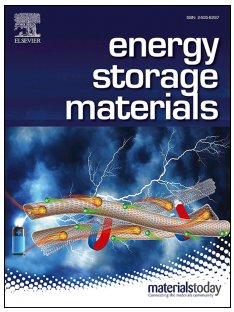

A Silicon Anode for Garnet-Based All-Solid-State Batteries: Interfaces and Nanomechanics

Weiwei Ping, Chunpeng Yang, Yinhua Bao, Chengwei Wang, Hua Xie, Emily Hitz, Jian Cheng, Teng Li, Liangbing Hu

PII: S2405-8297(19)30846-3

DOI: https://doi.org/10.1016/j.ensm.2019.06.024

Reference: ENSM 813

To appear in: *Energy Storage Materials*

Received Date: 6 December 2018

Revised Date: 10 June 2019

Accepted Date: 14 June 2019

Please cite this article as: W. Ping, C. Yang, Y. Bao, C. Wang, H. Xie, E. Hitz, J. Cheng, T. Li, L. Hu, A Silicon Anode for Garnet-Based All-Solid-State Batteries: Interfaces and Nanomechanics, *Energy Storage Materials*, https://doi.org/10.1016/j.ensm.2019.06.024.

A Silicon Anode for Garnet-Based All-Solid-State Batteries: Interfaces and Nanomechanics

Weiwei Ping,[1a] Chunpeng Yang,[1a] Yinhua Bao,[2a] Chengwei Wang,[1] Hua Xie,[1] Jian Cheng,[2] Emily Hitz,[1] Teng Li,[2*] Liangbing Hu[1*]

[1]Department of Materials Science and Engineering, University of Maryland, College Park, Maryland, 20742
[2]Department of Mechanical Engineering, University of Maryland, College Park, Maryland, 20742
[a] W.P., C.Y., and Y.B. contributed equally
[1*] Email: binghu@umd.edu
[2*] Email: lit@umd.edu

A Silicon Anode for Garnet-Based All-Solid-State Batteries: Interfaces and Nanomechanics

Weiwei Ping,[1a] Chunpeng Yang,[1a] Yinhua Bao,[2a] Chengwei Wang,[1] Hua Xie,[1] Emily Hitz,[1] Jian Cheng,[2] Teng Li,[2*] Liangbing Hu[1*]

[1]Department of Materials Science and Engineering, University of Maryland, College Park, Maryland, 20742
[2]Department of Mechanical Engineering, University of Maryland, College Park, Maryland, 20742
[a] W.P., C.Y., and Y.B. contributed equally
[1*] Email: binghu@umd.edu
[2*] Email: lit@umd.edu

Abstract

High-capacity electrode materials are indispensable for developing high energy density solid-state batteries. The lithium metal anode is attractive because of its high capacity and low electrochemical reduction potential, but its application is hampered by the dendrite issue. The silicon anode is a promising material having high capacity and invulnerability to undergoing dendrite formation, but is limited to the nanometer regime for the thickness of a Si anode. Herein, for the first time, we demonstrate a 1 μm thick solid-state silicon anode (10 times the typical thickness of Si anodes used in organic electrolyte) as an alternative to Li metal anode for solid-state batteries. This Si anode forms good contact with the garnet-type solid-state electrolyte and maintains structural integrity during the Li ion intercalation and extraction. The Si anode with the garnet electrolyte exhibits a high discharge capacity of 2685 mA h g^{-1} and an excellent initial Coulombic efficiency of 83.2%, higher than that of the Si anodes with an organic electrolyte (77.1%). Our mechanics modeling reveals that the strong nanomechanical constraints by the solid garnet electrolyte enables the substantial increase in the critical thickness of the Si anode from just nanometers to micrometers, toward high-capacity solid-state batteries.

Keywords: Solid-state battery, Silicon anode, Nanomechanics, Garnet, Modeling

Introduction

Solid-state batteries are promising candidates for the next-generation of safer and higher energy density Li-ion batteries.[1–7] Solid-state electrolyte (SSE) can provide potential solutions for many of the problems that have limited the development of liquid Li-ion batteries, such as flammability, limited voltage, unstable solid-electrolyte interphase formation, poor cycling performance and strength. Among them, $Li_7La_3Zr_2O_{12}$ (LLZO),[8–12] a garnet-type electrolyte is attractive because of its high ionic conductivity (~ 1 mS/cm),[13–15] wide electrochemical window (0-5 V), high shear modulus (~ 55 GPa),[16–18] and good chemical and thermal stability.

Lithium metal anode is one of the most promising anode materials for solid-state batteries with a theoretical specific capacity of 3860 mA h g^{-1}.[19–23] However, the utilization of Li metal anodes in solid-state batteries suffers from many issues including interfacial resistance and possible dendrite penetration,[24,25] which can lead to short-circuits. The Li-SSE interface resistance has been mitigated by various approaches, such as using a Li-Sn alloy,[26] modifying the solid-state electrolyte surface,[27–29] using polymer electrolyte as a buffer layer,[30] and cycling the battery at a low current density.[31] However, these solid-state cells were cycled at relatively small capacities under low current densities, 50-170 μA cm^{-2}.[11,26,30–32] The fundamental challenges associated with Li metal anodes in solid-state batteries have not been entirely eliminated by these methods, especially at high current densities and capacities. The dendrite growth along grain boundaries, especially at high current densities and high capacities, as well as those associated with the large volume expansion, could largely preclude the adoption of Li metal in future commercial solid-state batteries.[33–35]

Silicon anode features a higher theoretical capacity (~ 4200 mA h g^{-1}) than Li metal (~ 3860 mA h g^{-1}), making it a promising alternative to enable high energy density solid-state batteries without the issue of catastrophic dendrite formation due to the discharge voltage of Si.[36–39] However, the main challenge of using Si anodes in rechargeable batteries is its substantial volume change of up to 400% during lithiation and delithiation, which causes the electrode to crack and pulverize, resulting in poor interface with the electrolyte. To combat this problem, Si anodes in organic electrolyte are typically restricted to nanoscales (critical thickness ~100 nm),[40–44] which significantly limits the energy density of the battery. The recent development of solid-state electrolytes has presented potential solutions to many of the issues associated with liquid electrolyte Li-ion batteries. Moreover, Si anodes were recently explored with garnet-type SSE in 2018 by Ferraresi et al.[45] and Chen et al.,[46] but the thickness of these Si anodes is still in nanoscale (50 nm-180 nm), resulting in low energy densities of the battery.

Although low ionic and electronic conductivity can hinder the cycling and rate performance of thick electrodes,[47] it is well known that doping can significantly improve the electronic conductivity and lithiation improves the electronic and ionic conductivities of Si anodes.[48] However, a very limited number of studies seek to understand the interfacial and nanomechanical evolution of Si anodes in solid-state batteries, which is the critical obstacle to the practical implementation of solid-state Si anodes. In this work, by application of garnet-type SSE LLZAO ($Li_7La_3Zr_2O_{12}$ with 3 wt% Al_2O_3), we demonstrated a thick yet high-capacity Si anode, with critical thickness increasing from nanoscale to microscale regime. A solid-state Si anode of thickness 1 µm was successfully fabricated, which measures 10 times the thickness of Si anodes in organic electrolytes. We systematically investigated the morphology changes of the Si anodes with different thickness (1 µm, 2 µm, and 3 µm) in solid-state batteries and compared

the results, with corresponding Si anodes in liquid Li-ion batteries to gain an insight into the interface reaction properties of the solid-state Si anodes.

Results and discussion

As shown in the schematic (**Figure 1**a), during the lithiation process, Li ions transport across the garnet electrolyte from the Li metal and react with the Si anode to form Li_xSi. Our study shows that the 1 µm thick Si anode deposited via plasma-enhanced chemical vapor deposition (PECVD) shows amorphous structure (Figure S1) and mainly expands in the dimension normal to the garnet electrolyte without obvious crack formation either in the Si anode itself or at the Si/garnet interface. The garnet exhibits the cubic crystal structure and dense grain distribution with a high ionic conductivity of 4×10^{-4} S cm^{-1} (Figure S2, S3, and S4). As shown in Figure 1b, the deposited 1 µm Si anode is uniform and adheres to the garnet electrolyte. After the Li ions slowly diffuse through the garnet electrolyte and alloy with the Si anode, the Si anode expands, resulting in an increase in its thickness but no obvious cracks or pulverization after discharge (Figure 1c). The solid-state Si anode displays a high capacity of 2685 mA h g^{-1} (Figure 1d). Mechanics modeling also confirmed the advantage of the solid-state Si anode with the LLZAO electrolyte, which mitigates the structural damage of the Si anode by providing robust mechanical constraints that enable the Si anode to maintain its structural integrity during the lithiation/delithiation process. In this manner, we are able to achieve a thick 1 µm Si anode, ten times thicker than the Si anodes in organic electrolytes (100 nm).

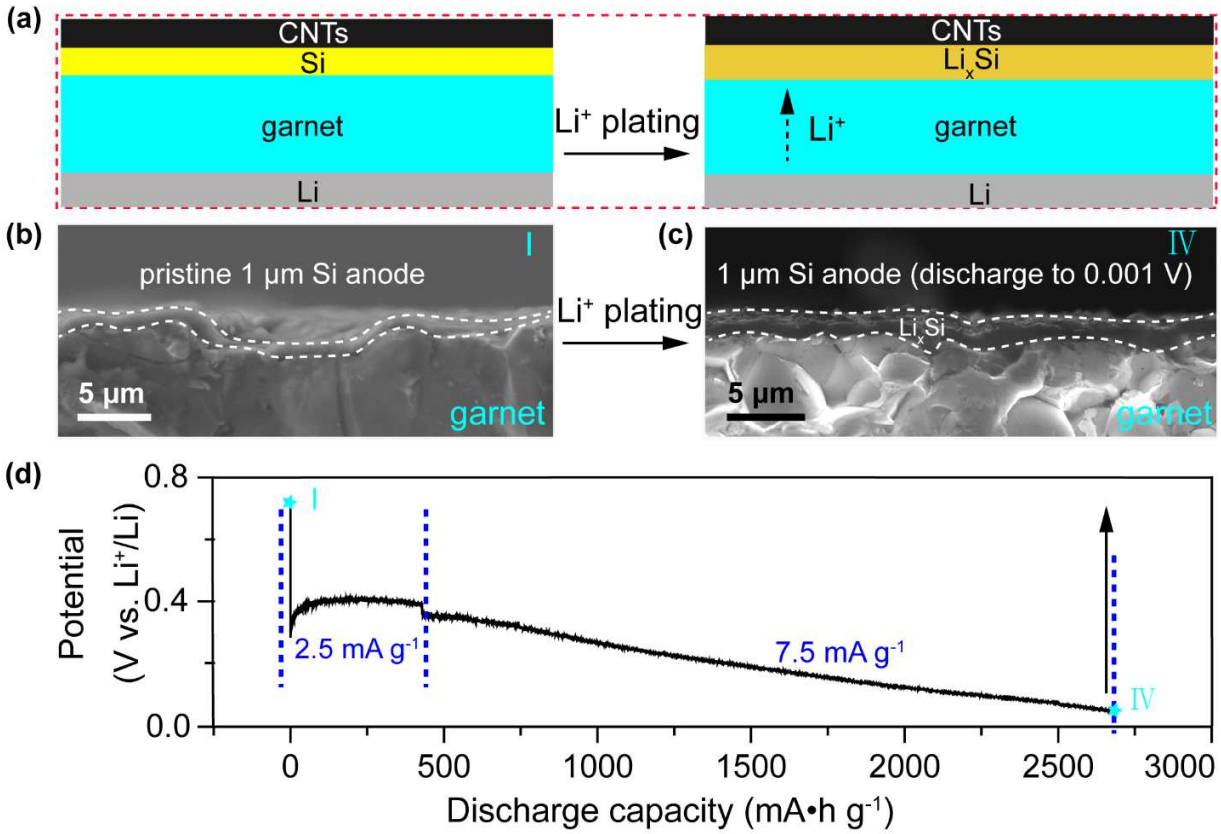

Figure 1. Morphology change of the Li/garnet/Si cell under discharging and the corresponding discharge curve. The thickness of Si anode is 1 μm, ten times the critical thickness of Si anode in organic electrolyte. A layer of carbon nanotubes (CNTs) was cast on the Si anode as a current collector. (a) Schematic of the Li plating process. Cross-sectional SEM images of the 1 μm Si anode (b) deposited on garnet by PECVD and (c) after discharging to 0.001 V. (d) Discharge profile of the solid-state Si anode.

We observed the morphology of the 1 μm thick Si film deposited on the solid-state LLZAO electrolyte using scanning electron microscopy (SEM) as shown in **Figure 2**a with a digital image of the anode displayed in the inset. A copper mask was employed during PECVD to control the deposition area to a 6 mm circular area and prevent deposition of Si on the LLZAO edges. The weight difference was measured to determine the mass of Si deposited. Mass loading

is calculated by dividing the mass by the area. During the deposition, the Si vapor deposited on the substrate uniformly with a grain size of about 500 nm (Figure 2a). Figure 2b exhibits the cross-sectional image of the Si anode on the garnet, demonstrating the continuous and dense Si film across the garnet pellet. High magnification cross-sectional SEM imaging and energy dispersive X-ray (EDX) spectroscopy mapping demonstrate that the Si film is uniformly coated on the garnet, with a dense and continuous structure and good interface contact (Figure 2c and 2d), which are vital for preventing the Si film from cracking during the volume change upon lithiation.

To overcome the solid-state Li ion transportation barrier, especially at the Si/garnet interface, a small current (2.5 mA g^{-1}, 7×10^{-4} mA cm^{-2}) activation process was utilized to slightly and smoothly intercalate Li ions into the solid-state Si anode. As shown in Figure 2e, after the activation process, the 1 μm thick Si anode exhibited high electrochemical activity. The Si anode delivers a discharge capacity of 2685 mA h g^{-1} (including a small irreversible capacity of ~ 90 mA h g^{-1} contributed by the CNTs, Figure S5) and a charge capacity of 2159 mA h g^{-1}, resulting in an initial Coulombic efficiency (ICE) of 83.2%. As a control experiment, we also studied the Si anode in liquid Li-ion batteries (Figure S6) with a conventional organic electrolyte, 1.0 M $LiPF_6$ in ethylene carbonate (EC) and diethyl carbonate (DEC), of which the electrochemical performance is also plotted in Figure 2e. The ICE of the Si anode in the liquid electrolyte was only 77.1%, indicating the reduced irreversible reactions at the interfaces of the solid-state Si anode. The electrochemical properties of the solid-state Si anode suggest the garnet and CNTs on the Si film provide a constraining effect that may help control the Si film volume change during battery cycling.

To get a more comprehensive and deep understanding of the Si/garnet interfaces during lithiation, we discharged solid-state Li/garnet/Si batteries to different states and then extracted the anodes to observe changes to the morphology. Control Si anodes on Cu substrates in liquid Li-ion batteries were also analyzed after discharge. As indicated in the discharge/charge voltage profiles in Figure 2e, the morphology evolution of the Si anode in the solid and liquid batteries were observed (i) before cell cycling and after the cells had been discharged to (ii) 0.2 V, (iii) 0.1 V, and (iv) 0.001 V. As shown in Figure 2f-i and Figure S7a, as the Li ions intercalated into the Si anode through the garnet SSE, the thickness of the Si anode increased from 1 μm (pristine, Figure 2f) to 1.2 μm (discharge to 0.2 V, Figure 2g), 1.55 μm (discharge to 0.1 V, Figure S7a), and finally 2.9 μm (discharge to 0.001 V, Figure 2h and 2i). Despite the thickness expansion, the Si anode remains strongly adhered to the garnet SSE without interface detachment or wrinkles, as shown in the large-scale SEM image of the cross section of the Li_xSi after discharging to 0.001 V (Figure 2i).

It is known that during the lithiation of amorphous Si and the formation of crystalline Li_xSi alloy, the Si anode undergoes crystallization and volume expansion.[49] During delithiation, the crystal Li_xSi becomes amorphous Si as the Si anode volume shrinks back. The high stress associated with continuous volumetric expansion-shrinkage process initiates cracking and pulverization of the anode, which is attributed to be the main reason for capacity decay.[50,51] However, with the garnet SSE in this work, the volume change of the Si on the garnet electrolyte was effectively constrained without obvious cracking and pulverization (Figure 2g-k and Figure S8c). SEM images (Figure 2j and 2k) of the discharge products (Li_xSi discharged to 0.001 V) from the surface of the anode also display a crack-free morphology. The volume expansion of the Si anode leads to Si particle growth, from ~ 500 nm for the pristine Si on garnet (Figure 2a)

to 1.41 μm for the Li_xSi discharge product (Figure 2j), but no cracking was observed in the Si anode after the 1st discharge (Figure 2h-j) or 2 cycles (Figure S8c and S8d).

In contrast, for Si anodes used in liquid batteries, the volume dilation associated with Li-Si alloying caused intense mechanical stress that led to the pulverization of the Si particles. When the cell Li/EC-DEC/Si/Cu was discharged to 0.001 V, the surface of the anode appeared rough and uneven, with many cracks and holes (indicated by white circles in Figure 2l). Inside the holes, obvious cracks in the Si anode are ubiquitous (indicated by circles in Figure 2m), which deteriorate the solid-electrolyte interface stability and Li ion transference, leading to a capacity decay.

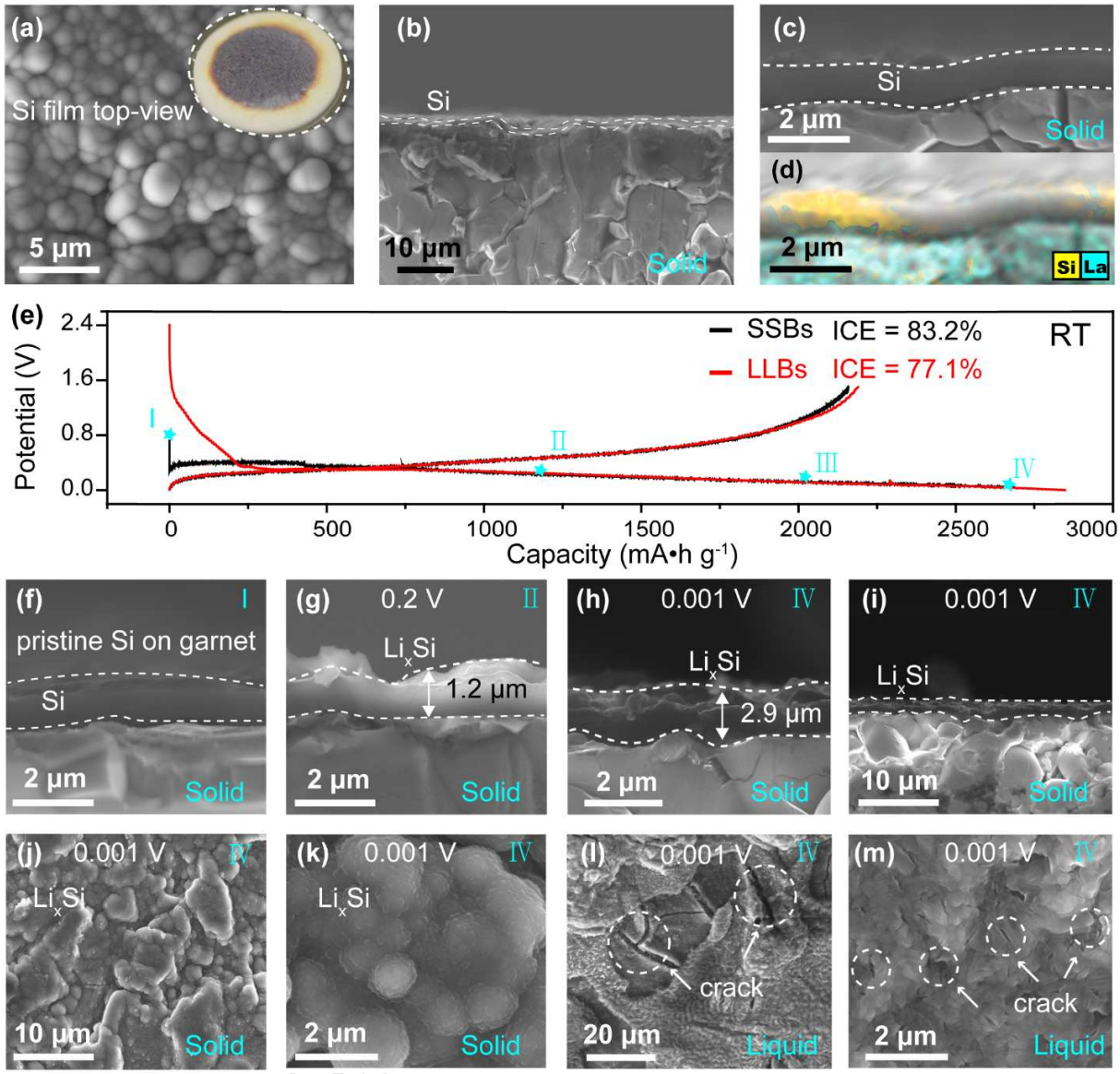

Figure 2. Morphology characterization and voltage profile of the 1 μm Si anode in solid-state and liquid Li-ion battery configurations. (a) Surface morphology (the inset image is the digital picture) and (b, c, f) cross-sectional SEM images of the 1 μm Si film deposited on garnet by PECVD at different magnifications, which indicates a conformal interface between the Si anode and garnet. (d) EDX mapping of the 1 μm Si film. (e) Voltage profile of the 1 μm Si anode in solid-state and liquid Li-ion batteries. Cross-sectional SEM images of the 1 μm Si anode discharging to (g) 0.2 V and (h, i) 0.001 V in solid-state configuration. Surface morphology of

the 1 μm Si anode after discharging to 0.001 V for the (j, k) solid-state and (l, m) liquid batteries at different magnifications.

To understand the effect of the thickness on the Si anode in the solid-state battery, we also investigated the morphology evolution of the material at greater thicknesses of 2 μm and 3 μm during lithiation. Similar to the 1 μm Si anode, the initial Si films were uniform and featured conformal contact with the garnet. After discharging to 0.2 V, no fractured layer can be seen in the 2 μm Si film and 3 μm film, and the Si/garnet interface remains intact, though the Si anode thicknesses increases slightly from 2 μm to 4 μm and 3 μm to 5.8 μm respectively.

However, when further discharging to 0.1 V, while the 2 μm Si anode remained tight contact with the garnet electrolyte (Figure S7b), the 3 μm Si anode became detached (Figure S7c). When fully lithiated (discharged to 0.001 V), the 2 μm Si anode exfoliates from the garnet without obvious cracks between the Si film and electrolyte, while the 3 μm Si anode separates from the garnet completely (**Figure 3**c and 3h). Under this condition, the surface of the 2 μm Si anode partially maintained its initial structure (Figure 3d) while the 3 μm Si anode became pulverized completely (Figure 3i). Figure 3j summarizes the thickness evolution of the 1 μm, 2 μm, and 3 μm Si anode at different discharge states. The 1 μm thick Si film demonstrates a smooth thickness increase during Li alloying, indicating moderate volume expansion of the Si anode. However, for the thicker Si anodes (2 μm and 3 μm), the boost in thickness during the initial discharge (to 0.2 V) could already lead to the anode exfoliation or pulverization. Therefore, the 1 μm Si anode delivers the highest capacity (2685 mA h g^{-1}), while the 2 μm Si anode exhibits a discharge capacity of 1713.8 mA h g^{-1}, and the 3 μm thick anode has only a capacity of 831.7 mA h g^{-1} (Figure S9). This could explain why the previous studies on solid-state Si anode were only based on thin Si films.

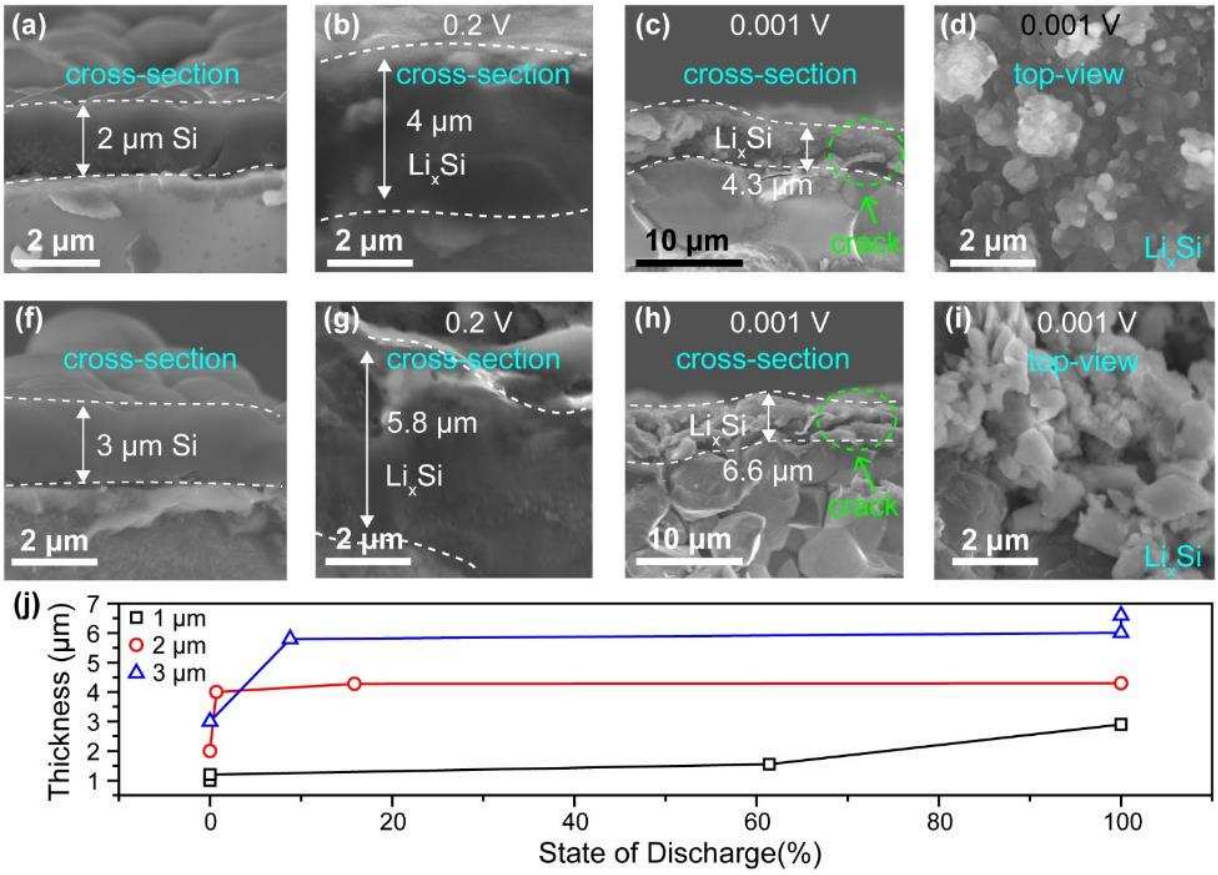

Figure 3. Cross-sectional SEM images of the (a) 2 μm and (f) 3 μm Si anodes deposited on garnet discharged to (b, g) 0.2 V and (c, h) 0.001 V. Surface morphology of the (d) 2 μm and (i) 3 μm Si anode after discharging to 0.001 V. (j) Thickness evolution profiles of the 1 μm, 2 μm, and 3 μm Si anode discharge to different states.

We further analyzed the electrochemical performance of the Si anode in the garnet-based all-solid-state battery using 1 μm thick Si, CNT current collector, and Li metal counter electrode. Figure 4a shows the first and second discharge/charge cycles at room temperature. The solid-state Si anode was first activated at low current of 2.5 mA g^{-1} (7×10^{-4} mA/cm²), and then cycled at the rate of 7.5 mA g^{-1} (2×10^{-3} mA/cm²). After the first cycle, the Coulombic efficiency further increases to 97.4%. The high Coulombic efficiency of the solid-state Si anode provides the all-solid-state battery with high reversibility. To further investigate the Si/garnet interface stability,

we performed cell impedance tests before cycling, after discharging, after charging, and after 2 discharge/charge cycles at room temperature (Figure 4b). After discharging, the impedance of the cell decreases from 475 Ω cm^2 to 323 Ω cm^2, suggesting that the ionic conductivity of the solid-state Si anode increases after Li insertion. In the subsequent delithiation and lithiation processes, the interface resistance featured only a slight change (374 Ω cm^2 after Li was extracted and 367 Ω cm^2 after the second lithiation), indicating the stable Si/garnet interface during electrochemical cycling.

Electrochemical impedance spectroscopy (EIS) of the solid-state Si anode was conducted at different temperature (from 20 ^oC to 80 ^oC) to understand the interface impedance and energy barrier (Figure 4c). We observed two semicircles at the high and medium frequency regions, which are associated with the total resistance from the garnet (R_1) and the interface between the Li and garnet (R_2), respectively. A nearly flat tail in the low-frequency region corresponds to the interface between the Si and garnet (R_3). The resistance of the garnet, Li/garnet, and Si/garnet interfaces decreased with increasing temperature. From the resistance-temperature dependence, we calculated the activation energies of the garnet and energy barriers at different interfaces according to the Arrhenius equation, which are plotted in Figure 4d. An activation energy of 0.39 eV was observed for garnet bulk, which is consistent with the literature.[28] It is intriguing that Li-ion transport energy barrier in the lithiated solid-state Si anode is only 0.24 eV, lower than that of the Li/garnet interface.[28,52] The lower energy barrier of Si suggests that it is easier for Li ions to migrate to the Si anode through the garnet compared with the Li metal anode, suggesting the Si is a feasible material for a solid-state battery anode.

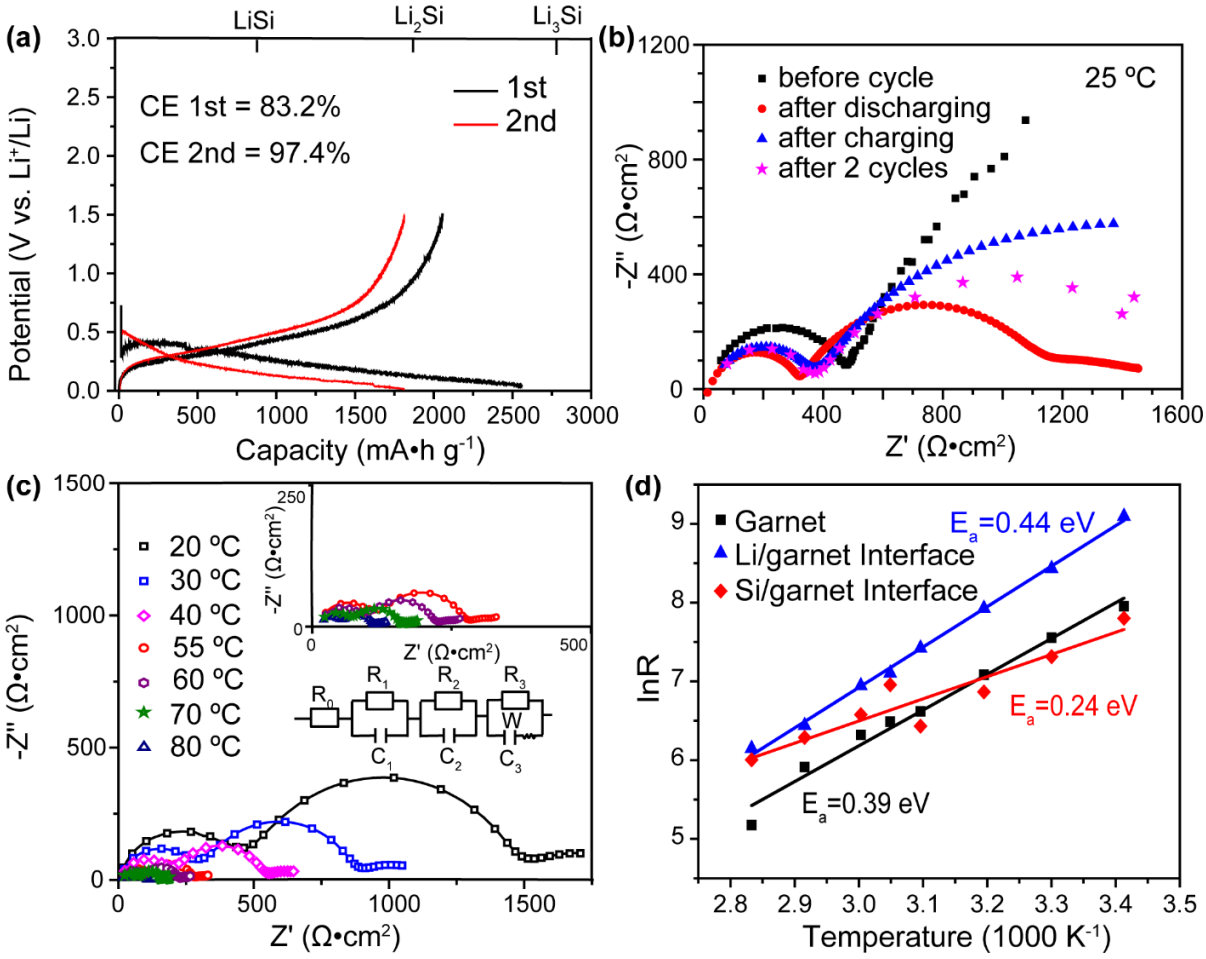

Figure 4. Electrochemical performance of the Li/garnet/Si cells featuring the 1 μm thick Si film. (a) Galvanostatic charge and discharge curves measured at room temperature. The cell was activated first with a current density of 2.5 mA g^{-1} (7×10^{-4} mA cm^{-2}) and then discharged at a current density of 7.5 mA g^{-1} (2×10^{-3} mA cm^{-2}). (b) Impedance measurements for the cell before electrochemical cycling, after discharge, after charge, and after second recharge. (c) EIS of the Li/garnet/Si cell at temperatures ranging from 20 ^{o}C to 80 ^{o}C; (d) Arrhenius plots of the resistance of the garnet, Li/garnet interface, and Si/garnet interface.

Experimentally, we have successfully fabricated 1 μm Si anodes with excellent electrochemical performance that are much thicker than many studies have used (~ 100

nm)[40,41] for liquid Li-ion batteries with organic electrolyte. Despite its thickness, the 1 μm Si anode kept its structural integrity and a tight contact to garnet electrolyte during Li plating/stripping process. We believe the high stiffness of the garnet is the main reason that the volume change of Si anode was effectively constrained during cycling to prevent mechanical degradation. To reveal the robust nanomechanical constraints of the garnet, we conducted finite element modeling based on the general Li ion concentration, stress distribution, and defective part in the 1μm Si anode (see details in the Supporting Information). The modeling results clearly show that both the Li ion concentration and stress distribution of the Si anode in the solid-state battery are relatively uniform along the Si film anode thickness direction during lithiation/delithiation, due to the slow charge rate and single-phase reaction of the Si anode film[53] (Figure S10 and S11). This uniform stress distribution and stable stress evolution effectively guarantee the overall structural stability of the Si anode. On the other hand, the in-plane stress of the Si anode periodically changes from compression to tension during charging/discharging, which is particularly severe at the Si anode surface (Figure S12), inducing fatigue fracture and crack propagation at relatively weak defective parts of the Si anode.

Furthermore, we revealed the nanomechanical advantage of the garnet by modeling the defective part of the Si anode (**Figure 5**). The simulation clearly captures the evolution of crack propagation in the Si anode with and without garnet (in solid-state and liquid Li-ion batteries) during the delithiation stage (Figure 5a, Figure 5c, Figure S13 and Supplementary movies 1 and 2). The large volume shrinkage leads to in-plane tensile stress in the Si anode. Once the tensile stress exceeds a critical limit, the crack initiates and propagates along the thickness direction. Constrained by the garnet electrolyte, the maximum crack opening displacement in the solid-state Li-ion batteries is much smaller than that in the liquid battery configuration at the full

delithiation state (Figure 5b), indicating the nanomechanical advantage of the solid-state electrolyte at mitigating structural damage to the Si anode. Moreover, the state of charge (SOC) when the crack initiates also decreases from 36% to 20%. The underpinning mechanism of the crack inhibition is also demonstrated by the crack dissipation energy in the Si anode. During the entire delithiation process, the smaller driving force for cracking is a crucial piece of evidence of the higher fracture resistance of Si anode with garnet (Figure 5d). Most critically, the strong Si/garnet interface effectively protects the Si anode by restraining adverse volume changes during lithiation and delithiation. Meanwhile, we theoretically analyzed the effect of the Si anode thickness on the electrochemical performance. The tunnel crack is considered as the major failure mode in Si anode during discharging/charging (Figure S14). The steady-state energy release rate for the tunnel crack increased linearly with the Si anode, which means that thicker Si anodes are more likely to crack during the delithiation stage (Figure S15). Comparing the mechanical state of the Si anode with and without garnet, the nanomechanical constraint of the garnet solid electrolyte clearly provides a remarkable enhancement of the electrode structural durability.

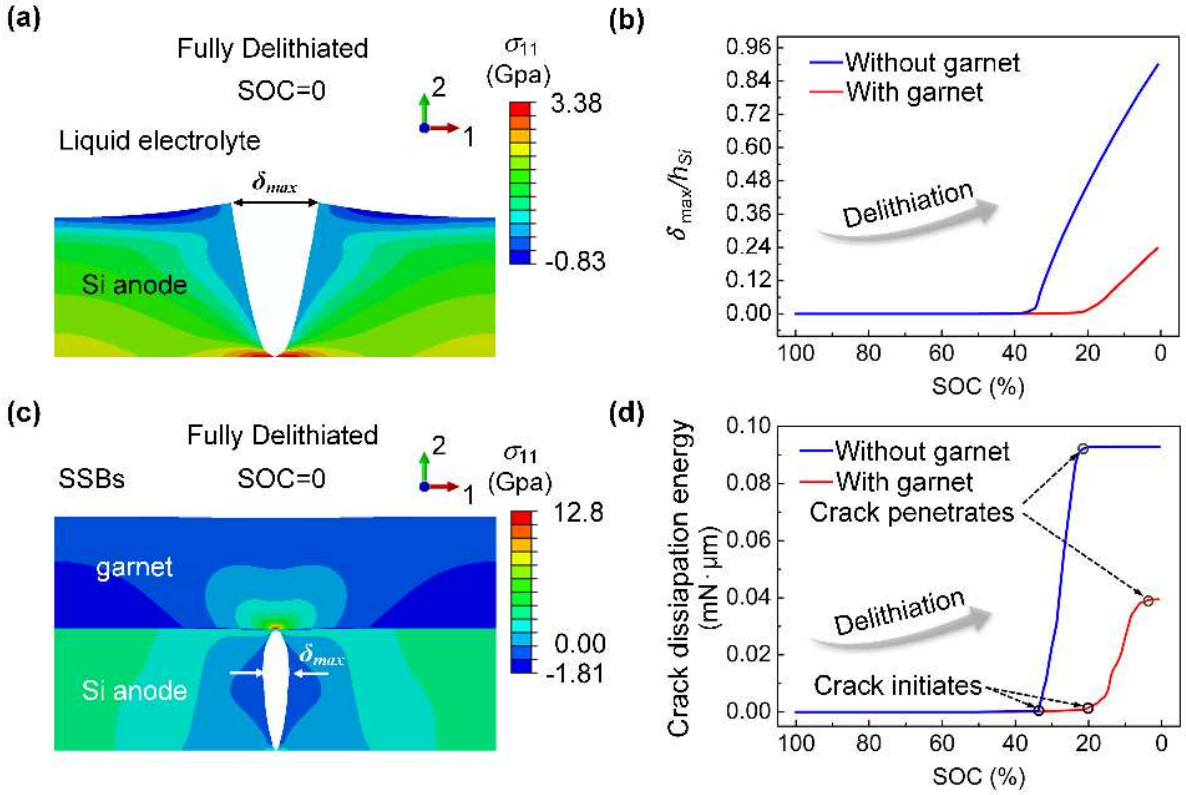

Figure. 5. Mechanical constraints of the garnet-type solid electrolyte. Finite element modeling of the morphology and normal in-plane stress distribution of the Si anode defective part in (a) liquid and (c) solid-state Li-ion batteries at the fully delithiated state. The color contours denote the in-plane stress (σ_{11}) level. (b) Comparison of the maximum crack opening displacement $\delta_{max}/2h_{Si}$ (normalized by the initial Si anode thickness h_{Si}) without (blue) and with (red) garnet during delithiation. (d) Comparison of the crack dissipation energy (mN·μm) in the Si anode without (blue) and with (red) garnet during delithiation.

Conclusion

For the first time, we have demonstrated a thick yet high capacity Si anode, with the thickness increasing from nanoscale to micro regime. The 1 μm thick Si anode was successfully fabricated in a garnet-type solid-state battery, and 10 times larger than the thickest amorphous nanoscale Si film (~100 nm) used for organic electrolytes. After an initial activation, the 1 μm Si anode in the solid-state battery shows a discharge capacity of 2685 mA h g^{-1} and high Coulombic efficiency of 83.2% at the first cycle, while the corresponding anode demonstrated only 77.1% ICE in organic electrolyte. We systematically investigated the interface and mechanical properties of the Si anode and garnet electrolyte during lithiation and delithiation. The interface between the Si anode and garnet maintains solid contact during this process, without creating any cracks or becoming pulverized. Based on our experimental and modeling results, we find that the strong nanomechanical constraint of the garnet leads to a substantially reduced volume expansion of the Si anode during lithiation. The garnet can also limit the Si film shrinkage during delithiation, preventing the anode from becoming damaged. Further work to improve ionic and electronic conductivities of the Si anode by doping or nano-engineering can be combined with the interface improvement to achieve better cycling and rate performances. We believe the present study on the interface and mechanics of the solid-state Si anode will trigger more interest in Si anode materials for high-energy density and durable solid-state batteries.

Experimental Section

Fabrication of the garnet solid-state electrolyte: Cubic garnet electrolyte composed of $Li_7La_3Zr_2O_{12}$ was fabricated via conventional solid-sate sintering. Stoichiometric amounts of LiOH (Alfa Aesar, 98.0%), La_2O_3 (Alfa Aesar, 99%), and ZrO_2 (Alfa Aesar, 99.9%) were weighed and thoroughly mixed with 3 wt% Al_2O_3 (Alfa Aesar, 99.0%) by ball milling for 24 h in polyethylene jars with isopropanol as media. 10 wt% Li was added to compensate for Li loss during the sintering process. After drying, the mixture was calcined at 1100 ^oC for 12 h. The as-calcined powder was broken down and pressed into disks 10 mm in diameter and 0.5 mm in thickness under a uniaxial pressure of 4.5 MPa. The pellets were then sintered in air at 1200 ^oC for 20 h. The pellets were polished on both sides prior to assembling into solid-state cells.

Si/CNT Anode fabrication and Soldering of Li: An amorphous Si film (~1 μm) was deposited by PECVD (Oxford Plasma Lab System 100) at 200 ^oC with the deposition rate of 25 nm/min and the power RF of 13.56 MHz. A gas composition of silane (SiH_4, 5%) and N_2 (95%) was used to do the deposition. Before deposition, the garnet was carefully polished by 1500 assorted grit sandpaper with isopropanol (IPA). Single wall carbon nanotubes (CNT) were dispersed into N-methyl-2-pyrrolidone (NMP) solvent under ultrasonic for 4h, with the concentration of 5 mg/mL. Then 10 μL CNT solution was dropped on the side of Si film by pipettes as the current collector. After drying on a 150 ^oC hot plate, the combine structure Si/CNT anode was achieved. To make the Li/garnet/Si cells for electrochemical measurements, Li foil was used as the counter/reference electrode by coating the Li-Sn alloy (30-50 wt% of Sn) on a hot plate at ~250 ^oC in an argon-filled glovebox.

Material Characterization: The morphology and particle size of Si before lithiation and delithiation and elemental mapping were observed by SEM (Hitachi SU-70) coupled with an EDS detector.

Electrochemical Measurement: Galvanostatic Si plating/stripping tests were performed on Bio-Logic MPG-2 battery cycler at room temperature. Electrochemical impedance spectra of the cells were tested on a Solartron electrochemical system in the frequency range of 1 MHz to 1 Hz and temperature range of 20 ^{o}C to 80 ^{o}C.

Finite element modeling: The lithiation/delithiation process and mechanical behavior of the Si anode was modeled through a fully coupled diffusion-displacement analysis in ABAQUS 6.13 (see details in Supporting Information). In the simulation, the bottom of the current collector was fixed, while the top and bottom surface of the Si film was tied to the current collector and LLZAO electrolyte, respectively. The displacement in the x direction was zero on the left and right side of the model. A nominal constant Li flux (0.0188 C) was given at the top surface of the Si anode according to the galvanostatic charging/discharging experimental results. The concentration dependent diffusivity was adopted in the model. Cohesive zone elements were implemented straight along the direction of the thickness of the anode to model the most likely crack penetration in the Si anode. The LLZAO/a-Si interface was also simulated by a cohesive zone model with strong interfacial toughness between them.

Supporting Information

Supporting information is available from the Wiley Online Library or from the author.

Acknowledgements

We acknowledge the support of the Maryland Nanocenter, its Surface Analysis Center and AIMLab. We acknowledge the University of Maryland supercomputing resources

(http://hpcc.umd.edu) made available for conducting the research reported in this paper. W. Ping acknowledges financial support by the China Scholarship Council (CSC).

Author contributions

L. Hu, W. Ping and C. Yang designed the experiments. T. Li, Y. Bao and J. Cheng performed simulations. C. Wang was responsible for Li coating on the garnet. H. Xie performed the garnet fabrication. L. Hu, W. Ping, C. Yang, T. Li, Y. Bao, and E. Hitz collectively wrote the paper. All authors commented on the final manuscript.

Reference:

[1] H. Ye, S. Xin, Y.X. Yin, J.Y. Li, Y.G. Guo, L.J. Wan, Stable Li Plating/Stripping Electrochemistry Realized by a Hybrid Li Reservoir in Spherical Carbon Granules with 3D Conducting Skeletons, J. Am. Chem. Soc. 139 (2017) 5916–5922.

[2] J.B. Goodenough, Y. Kim, Challenges for rechargeable Li batteries, Chem. Mater. 22 (2010) 587–603.

[3] D.G. Mackanic, W. Michaels, M. Lee, D. Feng, J. Lopez, J. Qin, Y. Cui, Z. Bao, Crosslinked Poly(tetrahydrofuran) as a Loosely Coordinating Polymer Electrolyte, Adv. Energy Mater. 8 (2018) 1.

[4] M. Armand, J.M. Tarascon, Building better batteries, Nature. 451 (2008) 652–657.

[5] E. Rangasamy, J. Wolfenstine, J. Sakamoto, The role of Al and Li concentration on the formation of cubic garnet solid electrolyte of nominal composition Li7La3Zr2O12, Solid State Ionics. 206 (2012) 28–32.

[6] R.L. Sacci, J.M. Black, N. Balke, N.J. Dudney, K.L. More, R.R. Unocic, Nanoscale imaging of fundamental Li battery chemistry: Solid-electrolyte interphase formation and preferential growth of lithium metal nanoclusters, Nano Lett. (2015).

[7] W. Li, Y. Yang, G. Zhang, Y.W. Zhang, Ultrafast and directional diffusion of lithium in phosphorene for high-performance lithium-ion battery, Nano Lett. (2015).

[8] J.F. Wu, W.K. Pang, V.K. Peterson, L. Wei, X. Guo, Garnet-Type Fast Li-Ion Conductors with High Ionic Conductivities for All-Solid-State Batteries, ACS Appl. Mater. Interfaces. 9 (2017) 12461–12468.

[9] X.X. Zeng, Y.X. Yin, N.W. Li, W.C. Du, Y.G. Guo, L.J. Wan, Reshaping Lithium Plating/Stripping Behavior via Bifunctional Polymer Electrolyte for Room-Temperature

Solid Li Metal Batteries, J. Am. Chem. Soc. 138 (2016) 15825–15828.

[10] M. Zarabian, M. Bartolini, P. Pereira-Almao, V. Thangadurai, X-ray Photoelectron Spectroscopy and AC Impedance Spectroscopy Studies of Li-La-Zr-O Solid Electrolyte Thin Film/$LiCoO_2$ Cathode Interface for All-Solid-State Li Batteries, J. Electrochem. Soc. 164 (2017) A1133–A1139.

[11] A. Sharafi, E. Kazyak, A.L. Davis, S. Yu, T. Thompson, D.J. Siegel, N.P. Dasgupta, J. Sakamoto, Surface Chemistry Mechanism of Ultra-Low Interfacial Resistance in the Solid-State Electrolyte Li7La3Zr2O12, Chem. Mater. 29 (2017) 7961–7968.

[12] E. Kazyak, K.H. Chen, K.N. Wood, A.L. Davis, T. Thompson, A.R. Bielinski, A.J. Sanchez, X. Wang, C. Wang, J. Sakamoto, N.P. Dasgupta, Atomic Layer Deposition of the Solid Electrolyte Garnet Li7La3Zr2O12, Chem. Mater. 29 (2017) 3785–3792.

[13] S. Afyon, F. Krumeich, J.L.M. Rupp, A shortcut to garnet-type fast Li-ion conductors for all-solid state batteries, J. Mater. Chem. A. 3 (2015) 18636–18648.

[14] R. Pfenninger, S. Afyon, I. Garbayo, M. Struzik, J.L.M. Rupp, Lithium Titanate Anode Thin Films for Li-Ion Solid State Battery Based on Garnets, Adv. Funct. Mater. 28 (2018) 1–8.

[15] J. Zheng, M. Tang, Y.Y. Hu, Lithium Ion Pathway within Li7La3Zr2O12-Polyethylene Oxide Composite Electrolytes, Angew. Chemie - Int. Ed. 55 (2016) 12538–12542.

[16] W. Xu, J. Wang, F. Ding, X. Chen, E. Nasybulin, Y. Zhang, J.G. Zhang, Lithium metal anodes for rechargeable batteries, Energy Environ. Sci. 7 (2014) 513–537.

[17] I. Garbayo, M. Struzik, W.J. Bowman, R. Pfenninger, E. Stilp, J.L.M. Rupp, Glass-Type Polyamorphism in Li-Garnet Thin Film Solid State Battery Conductors, Adv. Energy Mater. 8 (2018) 1702265.

[18] X. Zhang, T. Liu, S. Zhang, X. Huang, B. Xu, Y. Lin, B. Xu, L. Li, C.W. Nan, Y. Shen, Synergistic coupling between Li6.75La3Zr175Ta0.25O12and poly(vinylidene fluoride) induces high ionic conductivity, mechanical strength, and thermal stability of solid composite electrolytes, J. Am. Chem. Soc. 139 (2017) 13779–13785.

[19] J. Zheng, M.H. Engelhard, D. Mei, S. Jiao, B.J. Polzin, J.G. Zhang, W. Xu, Electrolyte additive enabled fast charging and stable cycling lithium metal batteries, Nat. Energy. 2 (2017) 17012.

[20] F. Ding, W. Xu, G.L. Graff, J. Zhang, M.L. Sushko, X. Chen, Y. Shao, M.H. Engelhard, Z. Nie, J. Xiao, X. Liu, P. V. Sushko, J. Liu, J.G. Zhang, Dendrite-free lithium deposition via self-healing electrostatic shield mechanism, J. Am. Chem. Soc. 135 (2013) 4450–4456.

[21] X.B. Cheng, R. Zhang, C.Z. Zhao, F. Wei, J.G. Zhang, Q. Zhang, A review of solid electrolyte interphases on lithium metal anode, Adv. Sci. 3 (2015) 1500213.

[22] Y.Y. Hu, Z. Liu, K.W. Nam, O.J. Borkiewicz, J. Cheng, X. Hua, M.T. Dunstan, X. Yu, K.M. Wiaderek, L.S. Du, K.W. Chapman, P.J. Chupas, X.Q. Yang, C.P. Grey, Origin of additional capacities in metal oxide lithium-ion battery electrodes, Nat. Mater. 12 (2013) 1130–1136.

[23] Y. Jin, K. Liu, J. Lang, D. Zhuo, Z. Huang, C. an Wang, H. Wu, Y. Cui, An intermediate temperature garnet-type solid electrolyte-based molten lithium battery for grid energy storage, Nat. Energy. (2018) 1–7.

[24] Y. Ren, H. Deng, R. Chen, Y. Shen, Y. Lin, C.W. Nan, Effects of Li source on microstructure and ionic conductivity of Al-contained Li6.75La3Zr1.75Ta0.25O12ceramics, J. Eur. Ceram. Soc. 35 (2015) 561–572.

[25] K. Ishiguro, H. Nemori, S. Sunahiro, Y. Nakata, R. Sudo, M. Matsui, Y. Takeda, O. Yamamoto, N. Imanishi, Ta-Doped Li 7 La 3 Zr 2 O 12 for Water-Stable Lithium Electrode of Lithium-Air Batteries, 161 (2014) 668–674.

[26] C. Wang, H. Xie, L. Zhang, Y. Gong, G. Pastel, J. Dai, B. Liu, E.D. Wachsman, L. Hu, Universal Soldering of Lithium and Sodium Alloys on Various Substrates for Batteries, Adv. Energy Mater. 8 (2017) 1701963.

[27] C. Yang, L. Zhang, B. Liu, S. Xu, T. Hamann, D. McOwen, J. Dai, W. Luo, Y. Gong, E.D. Wachsman, L. Hu, Continuous plating/stripping behavior of solid-state lithium metal anode in a 3D ion-conductive framework, Proc. Natl. Acad. Sci. (2018) 1–6.

[28] X. Han, Y. Gong, K. (Kelvin) Fu, X. He, G.T. Hitz, J. Dai, A. Pearse, B. Liu, H. Wang, G. Rubloff, Y. Mo, V. Thangadurai, E.D. Wachsman, L. Hu, Negating interfacial impedance in garnet-based solid-state Li metal batteries, Nat. Mater. 16 (2016) 572–579.

[29] N. Ohta, K. Takada, L. Zhang, R. Ma, M. Osada, T. Sasaki, Enhancement of the high-rate capability of solid-state lithium batteries by nanoscale interfacial modification, Adv. Mater. (2006).

[30] W. Zhou, S. Wang, Y. Li, S. Xin, A. Manthiram, J.B. Goodenough, Plating a Dendrite-Free Lithium Anode with a Polymer/Ceramic/Polymer Sandwich Electrolyte, J. Am. Chem. Soc. 138 (2016) 9385–9388.

[31] A. Sharafi, H.M. Meyer, J. Nanda, J. Wolfenstine, J. Sakamoto, Characterizing the Li-Li7La3Zr2O12interface stability and kinetics as a function of temperature and current density, J. Power Sources. 302 (2016) 135–139.

[32] Y. Li, X. Chen, A. Dolocan, Z. Cui, S. Xin, L. Xue, H. Xu, K. Park, J.B. Goodenough, Garnet Electrolyte with an Ultralow Interfacial Resistance for Li-Metal Batteries, J. Am.

Chem. Soc. 140 (2018) 6448–6455.

[33] V. Thangadurai, W. Weppner, Li6ALa2Ta2O12 (A=Sr, Ba): Novel garnet-like oxides for fast lithium ion conduction, Adv. Funct. Mater. 15 (2005) 107–112.

[34] Q. Lu, Y.B. He, Q. Yu, B. Li, Y.V. Kaneti, Y. Yao, F. Kang, Q.H. Yang, Dendrite-Free, High-Rate, Long-Life Lithium Metal Batteries with a 3D Cross-Linked Network Polymer Electrolyte, Adv. Mater. 29 (2017) 1604460.

[35] X.B. Cheng, R. Zhang, C.Z. Zhao, Q. Zhang, Toward Safe Lithium Metal Anode in Rechargeable Batteries: A Review, Chem. Rev. 117 (2017) 10403–10473.

[36] E.D. Mishina, K.A. Vorotilov, V.A. Vasil'ev, A.S. Sigov, N. Ohta, S. Nakabayashi, Porous silicon-based ferroelectric nanostructures, J. Exp. Theor. Phys. 95 (2002) 502–504.

[37] J. Sakabe, N. Ohta, T. Ohnishi, K. Mitsuishi, K. Takada, Porous amorphous silicon film anodes for high-capacity and stable all-solid-state lithium batteries, Commun. Chem. 1 (2018) 24.

[38] M. Pharr, K.J. Zhao, X.W. Wang, Z.G. Suo, J.J. Vlassak, Kinetics of Initial Lithiation of Crystalline Silicon Electrodes of Lithium-Ion Batteries, Nano Lett. (2012).

[39] H. Zhang, P. V. Braun, Three-dimensional metal scaffold supported bicontinuous silicon battery anodes, Nano Lett. (2012).

[40] J. Li, A.K. Dozier, Y. Li, F. Yang, Y.-T. Cheng, Crack Pattern Formation in Thin Film Lithium-Ion Battery Electrodes, J. Electrochem. Soc. 158 (2011) A689.

[41] J.P. Maranchi, A.F. Hepp, A.G. Evans, N.T. Nuhfer, P.N. Kumta, Interfacial Properties of the a-Si/Cu:Active–Inactive Thin-Film Anode System for Lithium-Ion Batteries, J. Electrochem. Soc. 153 (2006) A1246.

[42] M. Zhou, X. Li, B. Wang, Y. Zhang, J. Ning, Z. Xiao, X. Zhang, Y. Chang, L. Zhi, High-

Performance Silicon Battery Anodes Enabled by Engineering Graphene Assemblies, Nano Lett. (2015).

[43] S.C. Jung, J.W. Choi, Y.K. Han, Anisotropic volume expansion of crystalline silicon during electrochemical lithium insertion: An atomic level rationale, Nano Lett. (2012).

[44] T. Shimizu, T. Xie, J. Nishikawa, S. Shingubara, S. Senz, U. Gösele, Synthesis of vertical high-density epitaxial Si(100) nanowire arrays on a Si(100) substrate using an anodic aluminum oxide template, Adv. Mater. (2007).

[45] G. Ferraresi, M. El Kazzi, L. Czornomaz, C.L. Tsai, S. Uhlenbruck, C. Villevieille, Electrochemical Performance of All-Solid-State Li-Ion Batteries Based on Garnet Electrolyte Using Silicon as a Model Electrode, ACS Energy Lett. 3 (2018) 1006–1012.

[46] C. Chen, Q. Li, Y. Li, Z. Cui, X. Guo, H. Li, Sustainable Interfaces between Si Anodes and Garnet Electrolytes for Room-Temperature Solid-State Batteries, ACS Appl. Mater. Interfaces. 10 (2018) 2185–2190.

[47] W. Luo, Y. Gong, Y. Zhu, K.K. Fu, J. Dai, S.D. Lacey, C. Wang, B. Liu, X. Han, Y. Mo, E.D. Wachsman, L. Hu, Transition from Superlithiophobicity to Superlithiophilicity of Garnet Solid-State Electrolyte, J. Am. Chem. Soc. 138 (2016) 12258–12262.

[48] M.T. McDowell, Y. Cui, Single nanostructure electrochemical devices for studying electronic properties and structural changes in lithiated Si nanowires, Adv. Energy Mater. 1 (2011) 894–900.

[49] C.K. Chan, H. Peng, G. Liu, K. McIlwrath, X.F. Zhang, R.A. Huggins, Y. Cui, High-performance lithium battery anodes using silicon nanowires, Nat. Nanotechnol. 3 (2008) 31–35.

[50] H. Wu, G. Chan, J.W. Choi, I. Ryu, Y. Yao, M.T. Mcdowell, S.W. Lee, A. Jackson, Y.

Yang, L. Hu, Y. Cui, Stable cycling of double-walled silicon nanotube battery anodes through solid-electrolyte interphase control, Nat. Nanotechnol. 7 (2012) 310–315.

[51] N. Liu, Z. Lu, J. Zhao, M.T. Mcdowell, H.W. Lee, W. Zhao, Y. Cui, A pomegranate-inspired nanoscale design for large-volume-change lithium battery anodes, Nat. Nanotechnol. 9 (2014) 187–192.

[52] K.K. Fu, Y. Gong, B. Liu, Y. Zhu, S. Xu, Y. Yao, W. Luo, C. Wang, S.D. Lacey, J. Dai, Y. Chen, Y. Mo, E. Wachsman, L. Hu, Toward garnet electrolyte–based Li metal batteries: An ultrathin, highly effective, artificial solid-state electrolyte/metallic Li interface, Sci. Adv. (2017).

[53] X. Wang, S.S. Singh, T. Ma, C. Lv, N. Chawla, H. Jiang, Quantifying Electrochemical Reactions and Properties of Amorphous Silicon in a Conventional Lithium-Ion Battery Configuration, Chem. Mater. 29 (2017) 5831–5840.